SLEEPJ, 2022, 1–13

https://doi.org/10.1093/sleep/zsab204
Advance Access Publication Date: 10 August 2021
Original Article

ORIGINAL ARTICLE

Neuromodulation by means of phase-locked auditory stimulation affects key marker of excitability and connectivity during sleep

Georgia Sousouri[1,2], Elena Krugliakova[1], Jelena Skorucak[1], Sven Leach[1], Sophia Snipes[1,3], Maria Laura Ferster[2], Giulia Da Poian[2], Walter Karlen[2] and Reto Huber[1,4,*]

[1]Child Development Centre and Children's Research Centre, University Children's Hospital Zürich, University of Zurich, Zurich, Switzerland, [2]Mobile Health Systems Lab, Department of Health Sciences and Technology, ETH Zürich, Zurich, Switzerland, [3]Neural Control of Movement Lab, Department of Health Sciences and Technology, ETH Zürich, Zurich, Switzerland and [4]Department of Child and Adolescent Psychiatry and Psychotherapy, Psychiatric Hospital, University of Zürich, Zurich, Switzerland

*Corresponding author. Reto Huber, Child Development Center and Children's Research Centre, Uniersity Children's Hospital Zürich, Steinwiesstrasse 75, CH-8032 Zurich, Switzerland. Email: reto.huber@kispi.uzh.ch.

Abstract

The propagating pattern of sleep slow waves (high-amplitude oscillations < 4.5 Hz) serves as a blueprint of cortical excitability and brain connectivity. Phase-locked auditory stimulation is a promising tool for the modulation of ongoing brain activity during sleep; however, its underlying mechanisms remain unknown. Here, eighteen healthy young adults were measured with high-density electroencephalography in three experimental conditions; one with no stimulation, one with up- and one with down-phase stimulation; ten participants were included in the analysis. We show that up-phase auditory stimulation on a right prefrontal area locally enhances cortical involvement and promotes traveling by increasing the propagating distance and duration of targeted small-amplitude waves. On the contrary, down-phase stimulation proves more efficient at perturbing large-amplitude waves and interferes with ongoing traveling by disengaging cortical regions and interrupting high synchronicity in the target area as indicated by increased traveling speed. These results point out different underlying mechanisms mediating the effects of up- and down-phase stimulation and highlight the strength of traveling wave analysis as a sensitive and informative method for the study of connectivity and cortical excitability alterations.

Statement of Significance

Phase-locked auditory stimulation is a promising noninvasive tool to modulate ongoing brain activity during sleep. However, its mechanistic understanding remains elusive. We analyzed the traveling pattern of slow waves during auditory stimulation of their up and down phase. We demonstrate that up-phase stimulation mostly affects small waves by increasing their cortical involvement, propagating distance, and duration. On the other hand, down-phase stimulation interferes with traveling by disengaging cortical networks and increasing the traveling speed of large waves. These results may offer critical insights for personalized therapeutic applications of auditory stimulation in neurological and psychiatric disorders; slow-wave promotion could prove beneficial in age-related cognitive decline while desynchronization could prove valuable in reducing focal pathological synchronization as is the case in epileptic patients.

Key words: electrophysiology; slow-wave sleep; phase-locked auditory stimulation; slow-wave traveling

Submitted: 6 May, 2021; **Revised:** 15 July, 2021

Introduction

Slow waves (high-amplitude oscillations < 4.5 Hz) constitute a hallmark of electrical brain activity during nonrapid eye movement (NREM) sleep in surface electroencephalography (EEG). They have been shown to reflect slow oscillatory neuronal activity originating from an alteration of periods of neuronal silence (i.e., down states) and periods of increased synaptic activity (i.e., up states) [1, 2]. These slow oscillations can be generated and sustained alone in neocortical networks [3, 4], although thalamic oscillatory interactions exert modulatory effects [5]. In a high-density electroencephalography (hd-EEG) study in 2004, Massimini et al. [6] demonstrated that sleep slow oscillations can be modeled as traveling waves that periodically sweep the cerebral cortex and are characterized by a definite pattern of propagation. The authors showed that the traveling properties of slow oscillations are highly reproducible across nights and subjects and may serve as a blueprint of cortical excitability, brain connectivity, and local network activity [6–8]. Indeed, recently it was shown that propagation distance is an indicator of increased functional connectivity throughout healthy development [9] and that traveling distances and origin density are altered in schizophrenia. [10].

Sleep slow waves can be locally regulated in a use-dependent manner [2, 11, 12]. and are associated with mechanisms of synaptic plasticity [13], neuronal synchronicity, and cortical excitability [14, 15], playing an essential role in plastic learning processes [12, 16, 17]. Moreover, slow waves are thought to have beneficial effects on memory consolidation by facilitating synaptic activity underlying the encoding and storage of information and subsequent retrieval [18, 19].

Auditory stimulation is a noninvasive approach to modulate ongoing brain activity during sleep [20]. Studies indicate that the precise targeting of acoustic stimuli to the ascending phase of slow waves can enhance slow-wave activity (SWA, EEG power in the delta frequency range 1–4.5 Hz) on the single electrode level and can have beneficial effects on overnight memory retention [21–23] as well as encoding-related hippocampal activation [24]. Furthermore, sleep enhancement through auditory stimulation has been shown to successfully promote restorative functions of sleep by enforcing immune-supportive processes and enhancing parasympathetic activity [25, 26]. Conversely, in a hd-EEG study, targeted auditory stimulation at the descending slope of slow waves resulted in a local decrease of SWA close to the detection area, which was associated with reduced capacity to undergo motor learning [16]. The high potential of this neuromodulatory approach is indicated by recent studies showing that enhancement of slow oscillations via auditory stimulation might have a therapeutic potential in mild cognitive impairment and attention deficit hyperactivity disorder [27, 28]. Moreover, also the reduction of SWA might have therapeutic potential, e.g. in epilepsy where local neuronal network desynchronization could interfere with pathological spike-wave activity in sleep [29]. However, the underlying mechanisms of this approach remain unknown. Therefore, the analysis of the modulation of the spatiotemporal dynamics of slow-wave-sleep oscillations may provide novel insights.

In this work, we examine for the first time how the traveling pattern of slow waves is affected by the application of phase-locked auditory stimulation in both the up and down phases of sleep slow waves in a right prefrontal area. Based on previous findings, we hypothesized that phase-targeted auditory stimulation at the up-phase of slow waves would promote their propagation pattern, whereas down-phase perturbation would locally interfere with this pattern. We demonstrate local changes in key traveling parameters which contribute to the mechanistic understanding of this promising intervention tool.

Methods

Participants

Eighteen healthy, right-handed subjects in the age range between 21 and 26 years (mean±sem; standard error of the mean, age: 23.6 ± 1.5 years old, 9 females) participated in this study. Subjects were instructed to keep a constant sleep-wake schedule for ~7 days (range from 4–8 days) preceding the experimental session which was assessed using daily sleep diaries and wrist actigraphy monitoring (Actiwatch Type AWL, CamNtech, Cambridge, UK). Participants did not take any medication during the experiment and were required to refrain from alcohol, caffeine and any other medical and recreational drug 24 hours prior to the experimental session. Written informed consent was obtained prior to participation. The study was approved by the cantonal ethics committee (Kantonale Ethikkommission Zürich, KEK-ZH) and performed in compliance with the Declaration of Helsinki. Of the eighteen recorded subjects, seven were excluded from further analyses due to the following reasons: poor quality of sleep EEG data in one or more sessions (low sleep efficiency; four subjects), missing data from one session due to dropout (one subject) and low number of stimulations and/or detected traveling waves (three subjects). Data from ten participants (mean ± sem age: 23.7 ± 0.5 years old, all right-handed, 6 females) are included in subsequent analyses.

High-density sleep electroencephalography

All night hd-EEG recordings were collected (Electrical Geodesics Sensor Net for long-term monitoring, 128 channels, Net Amps 300 series, Electrical Geodesics Inc., EGI, Eugene, OR). Electrooculographic (EOG) and submental electromyographic (EMG) recordings were used for visual sleep scoring. Two additional electrodes (gold, Grass Technologies, West Warwick, RI) were attached to the earlobes, which served as reference for the traveling-wave detection. After adjusting the net to the vertex and the mastoids, all electrodes were filled with an electrolyte gel (ECI Electro-Gel, Electro-Cap International, Inc., Eaton, OH) to ensure high conductance for the maintenance of good signal quality throughout the night. EEG electrode impedances were below 50 kΩ at the start of the recording and were controlled again in the morning. All channels were referenced to Cz and signals were sampled at 500 Hz.

Experimental protocol

All subjects participated in three experimental nights that were separated by 1 week: 1) auditory stimulation with tones delivered during the ascending phase of sleep slow waves (Stim Up), 2) auditory stimulation with tones delivered during the descending phase of sleep slow waves (Stim Down), and 3) no stimulation was applied (Sham). The order of the three experimental nights was randomized and counterbalanced across subjects.

Real-time phase-locked auditory stimulation

We used a configurable mobile EEG system (MHSL-SleepBand; MHSL-SB) [30] for real-time slow-wave detection and phase-locked auditory stimulation. Stimulation triggers of the MHSL-SB were sent as digital input to the EGI amplifier and thus, the output of the MHSL-SB was mapped on the hd-EEG trace. For the MHSL-SL three gold electrodes were placed such that the detection electrode was attached to the right forefront of the head (between electrodes 2 and 9 of the hd-EEG, near the Fp2 location according to the standard 10–20 system) to monitor EEG activity in real-time. Two additional electrodes were attached to the mastoids, which served as the ground (contralateral to the detection electrode) and the reference (ipsilateral to the detection electrode). Finally, a set of headphones (sleepPhones, AcousticSheep LLC, Peninsula Drive, Pennsylvania) was taped to the ears of the subject for the delivery of acoustic stimuli.

A detailed description of the MHSL-SB algorithm can be found in [30]. Briefly, three binary classifiers were running in parallel: 1) a sleep detection classifier that was continuously evaluating delta and muscle (high beta) EEG power; if predefined power thresholds were met, sleep detection was satisfied, 2) a SWA classifier that was continuously evaluating delta power; if a predefined power threshold was met, SWA detection was satisfied and 3) a phase detection classifier using a phase-locked loop (PLL) architecture to estimate the phase of the input EEG signal; for Stim Up, when the estimated phase reached 35° (0° corresponds to positive zero-crossing), the phase condition was satisfied; for Stim Down, when the estimated phase reached 245°, the phase condition was satisfied. Our aim was to stimulate during the transition to the up- and the down-state, respectively. Due to the differences in properties of positive and negative half-waves (e.g., amplitude, slope, etc.) the PLL parameters differed between Stim Up and Stim Down in order to minimize the phase detection error for each condition. When all three conditions (sleep, SWA, and phase detection) were satisfied, an auditory stimulus (50 ms tone of pink 1/f noise, 50 dB) was delivered via the headphones. The stimulation was applied in windows of 6 s (ON windows). Each ON window was followed by a 6-s window where no stimulations occurred (OFF windows). An exact offline replication of the MHSL-SB algorithm on the EEG data provided the specific timing of stimulations (hypothetical tones) that would have occurred during the OFF windows and the Sham session. Due to the different PLL parameters selected for the optimization of the up versus down phase detection, the EEG of the Sham session was processed in two ways; one providing the hypothetical tones at the ascending phase of the slow waves (Sham Up) and one providing the hypothetical tones at the descending phase of the slow waves (Sham Down) to enable the comparison with the respective Stim sessions. Stimulation was applied during the first 2.5 hours after the delivery of the first tone, whereas SWA is maximum and we would obtain the strongest effects as also shown in previous studies [20]. A summary of the stimulation parameters is shown in Table 1.

Table 1. Summary of stimulation parameters

	UP		DOWN	
	Sham	Stim	Sham	Stim
Nr. of stimulations	1468 ± 114	1452 ± 110	1277 ± 95	1124 ± 137
Tone volume (dB)	0	50	0	50
Phase targeting (°)				
Mean	35	34.6	244.9	246.4
SD	43.7	40.4	45.7	48

Mean number of stimulations, tone volume intensity and mean phase targeting at detection electrode (channel 2 in hd-EEG) across sessions for both UP and DOWN conditions.

Sleep scoring and artifact removal

Sleep EEG was low-pass filtered at 40 Hz using the default FIR filter implemented in EEGLAB v14.1.1 [31] (least squares, two-way zero-phase, filter order: 36, cut-off frequency (–6 dB) at 42.8 Hz), high-pass filtered at 0.5 Hz (least squares, two-way zero-phase, filter order: 3000, cut-off frequency (–6 dB) at 0.46 Hz) and then down-sampled to 128 Hz. Sleep stages were visually scored for 20 second epochs according to standard criteria [32] by a sleep expert and verified by another sleep expert (both blind to the experimental conditions). In addition to a visual detection of artifacts during sleep scoring, a visual semiautomatic procedure was followed to detect artifacts based on average power values of the EEG signals [33].

Data preprocessing

Only data from the first 2.5 hours after the first tone were used for analysis. All signals were high-pass filtered at 0.1 Hz (EGI filter) to remove the dc offset. We notch-filtered the data at 50 Hz as well as at all harmonics up to 150 Hz to remove line-noise using a FIR filter (kaiser window, two-way zero-phase, filter order: 560, cut-off frequencies (-6 dB) at 47 and 53 Hz). Then, we low-pass filtered the data at 40 Hz using the default FIR filter implemented in EEGLAB v14.1.1 [31] (Hamming window, one-way zero-phase, filter order: 166, cut-off frequency (–6 dB) at 45 Hz) and finally re-referenced to the average of the two earlobe channels. 19 channels located on the neck and cheek were excluded and 109 channels were retained for further analysis.

Traveling-wave analysis

For the analysis of the traveling waves (TWs) we adapted the method described in [34] using a composite reference signal for the detection of TWs. A key adaptation to this method was the selection of the involved channels in the slow-wave traveling by computing the magnitude squared coherence [35, 36], a measure of spectral coherence connectivity. Moreover, we used the prototypical channel instead of the artificial composite signal for the slow-wave detection and the computation of the coherence (see slow-wave detection and channel involvement).

Slow-wave detection

To create a single reference for the timing of the occurrence of each TW a composite signal was generated by all the earlobe-referenced EEG signals, as previously described [34, 37, 38]. This method provides the advantage of capturing both local and more global events [34]. Specifically, all preprocessed signals were high-pass filtered at 0.5 Hz (equiripple FIR filter design using the Parks-McClellan algorithm, one-way zero-phase, filter order: 3876, cut-off frequency (–6 dB) at 0.34 Hz) and the

negative envelope was calculated by selecting the fifth most negative sample across all channels. The resulting reference signal was low-pass filtered at 4 Hz (equiripple FIR filter design using the Parks-McClellan algorithm, two-way zero-phase, filter order: 1287, cut-off frequency (–6 dB) at 4.6 Hz). A slow-wave detection procedure was applied to the filtered (0.5–4 Hz) reference signal based on consecutive zero crossings. We introduced a minimal dynamic amplitude threshold to select slow-wave negative peaks. For each subject, we computed the median absolute deviation (MAD) of the amplitudes of all local minima of the reference signal belonging in N3 epochs. That deviation was multiplied by a factor of 5 and the median absolute amplitude of the negative peaks was added. Finally, that value divided by 10 gave the minimum amplitude threshold for each subject [34]:

$$AmpThres_i = \frac{5 \cdot MAD\,(A_i) + median(A_i)}{10}, \quad (1)$$

where $AmpThres_i$ denotes the subject-specific minimum amplitude threshold and A_i the amplitudes of all local minima of the reference signal belonging in N3 epochs for subject i. An additional maximum threshold excluded all local minima exceeding –500 μV. Since both the zero crossings and the positive peaks of the reference signal do not provide meaningful information (they are resulting from the fifth most negative samples of the overlapping EEG signals), we used the local minimum between each pair of consecutive downward and upward zero crossings as a reference point centered around a 400 ms window in order to identify the actual EEG channel that recorded the largest negative peak (i.e., the prototypical channel). Next, we computed the duration of the negative prototypical halfwave which should be between 125 and 1000 ms, corresponding to slow waves with a frequency of 0.5 to 4 Hz. This frequency range was selected for the prototypical wave detection, since it is the frequency range used by the MHSL-SB SWA classifier.

Channel involvement

As a next step, we computed the channel involvement, that is, which channels were recruited at each cycle of the slow oscillation, using a measure of functional connectivity based on spectral EEG coherence which quantifies the extent of synchronicity between two stationary signals at a specific frequency f [35, 36]. We computed the magnitude squared coherence, using Welch's averaged modified periodogram method [39] on the broadband (0.5–40 Hz) filtered signal, between the prototypical wave (i.e., the wave with the largest negative peak and thus most prominent in each cycle of the TW) and every other EEG signal at all electrode sites. The magnitude squared coherence $C_{x,y}(f)$ for two signals x and y in a specific frequency f is defined as:

$$C_{x,y}(f) = \frac{|P_{x,y}(f)|^2}{P_{x,x}(f) \cdot P_{y,y}(f)} \quad (2)$$

with $P_{x,x}(f)$ and $P_{y,y}(f)$ denoting the auto-power spectral density estimates of x and y, respectively, and $P_{x,y}(f)$ the cross-power spectral density estimate of x and y. For the coherence estimates, we used EEG data segments of 1 s centered around the negative peak of the prototypical channel and zero-padded to 2 seconds. We used a sliding Hanning window of 1 s with 50% overlap and a frequency resolution of 0.25 Hz. The channels that showed higher (> 0.75, range: 0–1) coherence with the prototypical channel in the delta frequency band (0.5–4 Hz) were identified. In a second step, a cluster analysis based on neighboring electrodes was performed on the resulting involvement topography in order to identify and exclude island electrodes of probable artifactual origin. Next, we computed the amplitude of the negative peak of the EEG segment at each remaining electrode, and the waves with amplitudes smaller than the previously described minimum amplitude threshold in Equation (1) were discarded from the involvement distribution. The delays of the negative peaks of the remaining channels were computed with respect to the origin, i.e. the channel that first recorded the negative peak (t = 0 seconds). Delay values were normalized for each subject by centering around the mean.

Traveling-wave propagation

As a final step, the propagating pattern of the TWs was computed by calculating a set of streamlines based on the evaluation of the continuity of the gradient of the delays [34]. The delay values of all the involved electrodes were interpolated into a two-dimensional (2D) cartesian grid (40 x 40) to create a delay map summarizing the information about the temporal and spatial distribution of the slow oscillation. The gradient of the delays was evaluated at each point and three conditions indicated the stopping of a streamline: 1) nonexisting gradient at the next point, indicating no slow wave was recorded at the corresponding site, 2) change in gradient angle greater than 90°, indicative of counteracting gradients and, 3) gradient equal to zero, corresponding to a stop of the traveling of the slow-wave. Several streamlines are calculated for each wave, however, a subset of three streamlines is saved for each wave: 1) the streamline with the longest displacement (i.e. the biggest Euclidean distance from start to end-point), 2) the streamline with longest distance traveled (i.e., the cumulative sum of all coordinates of the line) and, 3) the streamline with most angular deviation from the longest displacement (see Figure 1B). The first streamline was used for the analysis (see last part of traveling-wave selection procedure). Mean number of all detected TWs is shown in Table 2.

Traveling-wave selection procedure

Investigation of the changes in the slow-wave traveling after phase-locked auditory stimulation during the up and down phase of slow waves was performed in three steps.

1) First, the overall induced changes on the topographical traveling characteristics due to stimulation were assessed. Therefore, the following procedure was applied:

(i) All the waves in which their prototypical negative peak belonged to ON and OFF windows in which at least three stimulations occurred (or would have occurred, respectively) were included in the analysis. Consequently, OFF periods were not always following an ON period and vice versa. The selection was independent of whether the individual wave was stimulated or not (see Figure 2A). Mean number of selected TWs is shown in Table 2.

(ii) We computed the changes in traveling by directly comparing the waves in the ON to the waves in the OFF windows within a session (i.e., for the involvement we computed the ON/OFF ratio for each electrode, indicated as ΔStim and ΔSham). This direct intra-night ON/OFF comparison

is advantageous by avoiding the effects of night-to-night differences that could mask any intervention effects when directly comparing to Sham. In order to investigate after effects, we compared the OFF windows between conditions and did not see any changes (data not shown).

(iii) As a next step, we assessed the effect of the auditory stimulation in Stim as compared to Sham sessions by contrasting the resulting ON/OFF ratio in Stim to the respective ON/OFF ratio in Sham (indicated as ΔStim/ΔSham for the up- and down-phase stimulation, respectively).

(iv) Finally, we moved to a direct comparison between the up- and down-phase stimulation by contrasting $(\Delta Stim/\Delta Sham)_{UP}$ to $(\Delta Stim/\Delta Sham)_{DOWN}$ indicated as ΔUP/ΔDOWN.

2) At a second step of the analysis, only the TWs that got stimulated (or would have been stimulated in OFF windows and Sham sessions) were selected in order to elucidate the direct effect of the stimulation on the traveling of the individual waves.

(i) For the up-phase stimulation, the waves that had an auditory stimulus during the ascending slope of the

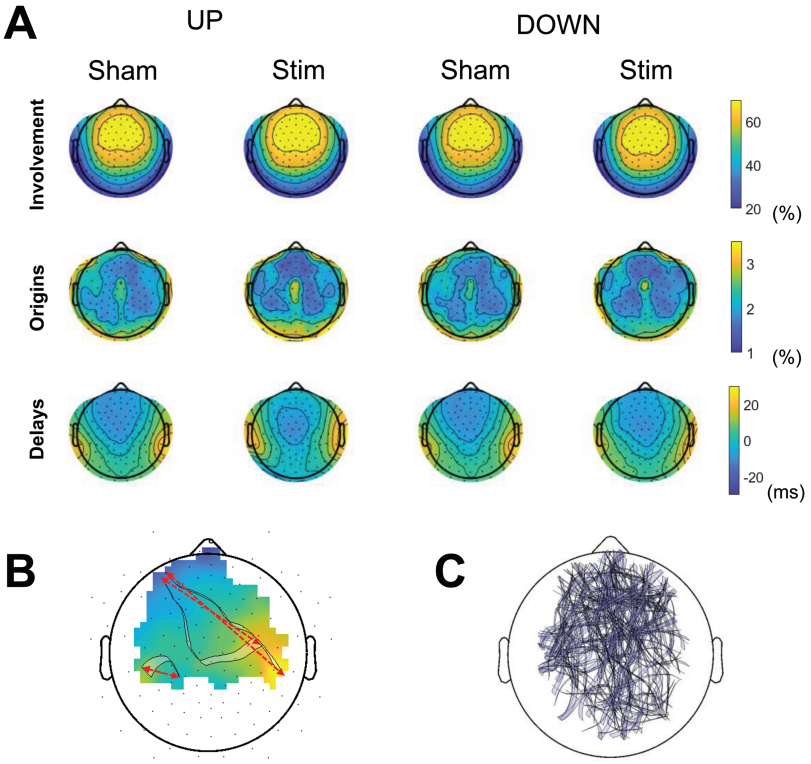

Figure 1. Topography of traveling-wave characteristics. A) Grand average topographical maps of the major characteristics of TWs reproducible across sessions. All TWs detected in ON and OFF windows are selected here. Upper row: cortical involvement topographical maps representing the probability of each channel being recruited in a traveling oscillation. Higher involvement probability for broad frontal areas. Middle row: origin density maps showing the probability of each channel being the origin of a TW. Higher probability for orbitofrontal and central areas. Bottom row: Delay maps displaying the prevalent direction of propagation from frontal to occipital cortical regions. B) Topographical representation of a representative traveling wave with computed streamlines superimposed. The colored part of the head plot represents the cluster of channels that detected a negative slow-wave peak (i.e., the channels that were involved in the traveling—"involvement") and the colors correspond to their respective interpolated "delays" (small delays represented with blue and big delays with yellow color). The three streamlines that resulted from the TW propagation analysis are superimposed. Streamline width reflects change of direction. We may note that the starting points of the streamlines are located in the regions with small delays and their trajectory follows the gradually increasing path of the delays. The red dashed lines from the starting point of each streamline to their respective ending points represent the total "displacement" of each streamline. C) Example of a streamline map. The preferred propagation along the antero-posterior axis can be distinguished.

Table 2. Mean number of traveling waves (TWs) at each step of the analysis

	UP				DOWN			
	Sham		Stim		Sham		Stim	
Initial no. of TWs	2542 ± 194		2560 ± 316		2579 ± 201		2448 ± 269	
	ON	**OFF**	**ON**	**OFF**	**ON**	**OFF**	**ON**	**OFF**
>3 stims	1109 ± 94	1113 ± 88	1171 ± 131	1158 ± 141	1078 ± 93	1071 ± 94	1030 ± 110	1009 ± 103
Small TWs	177 ± 16	177 ± 14	160 ± 20	202 ± 23	141 ± 15	145 ± 16	109 ± 13	142 ± 19
Large TWs	301 ± 27	297 ± 27	382 ± 47	277 ± 34	333 ± 35	328 ± 36	324 ± 4	286 ± 31
Right prefrontal TWs	277 ± 28	288 ± 30	328 ± 42	321 ± 39	336 ± 36	339 ± 39	321 ± 42	326 ± 38
Left prefrontal TWs	178 ± 25	176 ± 23	189 ± 27	174 ± 23	200 ± 30	199 ± 26	163 ± 24	182 ± 26

Initial no. of TWs: number of TWs right after the TW detection; >3 stims: number of TWs that belonged in windows with more than three stimulations; Small TWs: number of small TWs; Large TWs: number of large TWs; Right/left prefrontal TWs: number of TWs that were detected in the right/left prefrontal area.

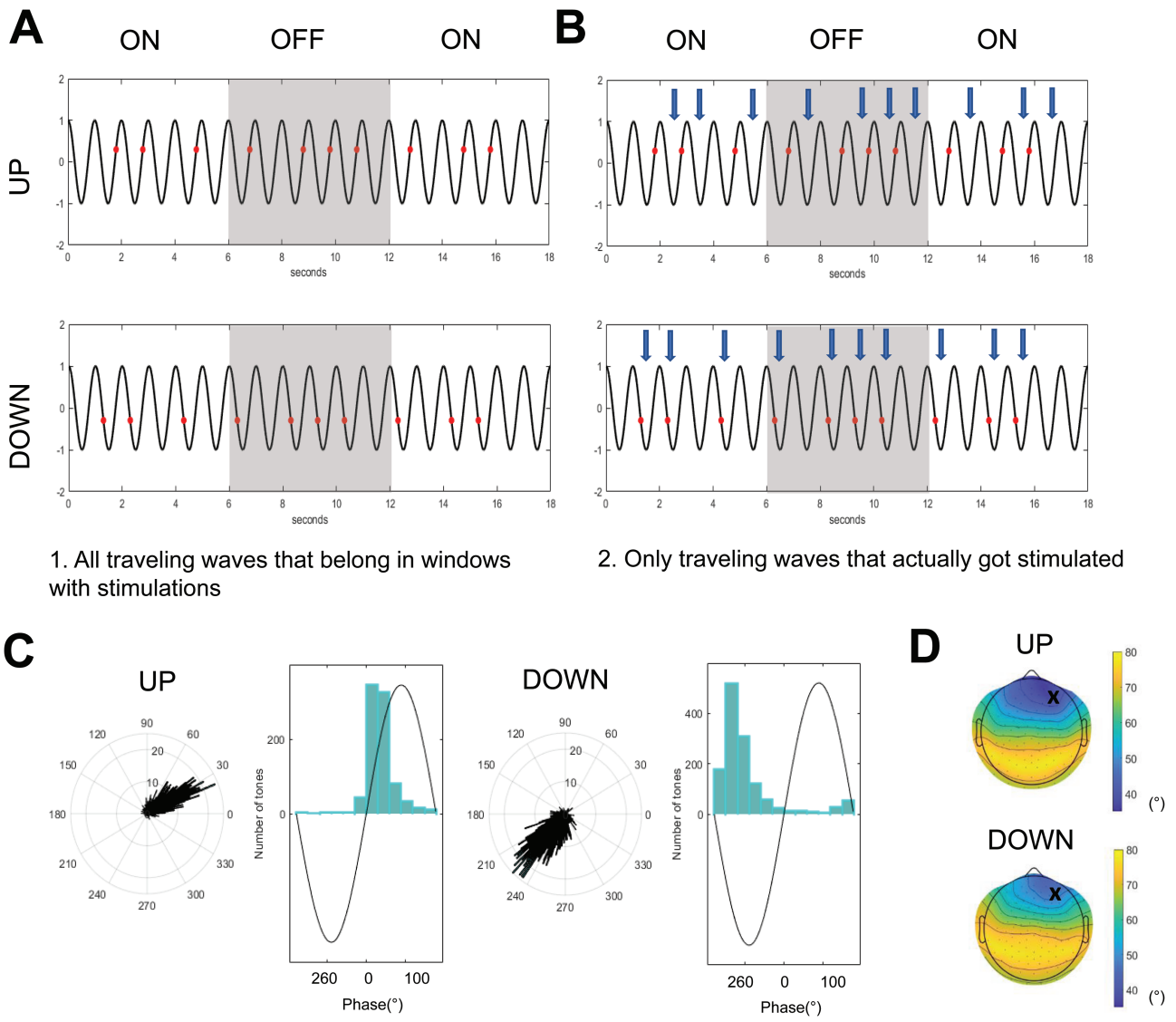

Figure 2. Methods and stimulation performance. A) Representation of the TW selection procedure at the first part of the analysis for both conditions (UP and DOWN). Sinusoids represent detected waves and red dots represent stimulation tones. B) Representation of TW selection procedure where only TWs during which a stimulation took place were selected. These are highlighted with blue arrows. C) Representative histograms from a single recording of phase targeting accuracy in the detection electrode (channel 2 on hd-EEG) for both conditions (UP and DOWN) of the same participant. D) Topographical distribution of the circular standard deviation of phase targeting for both conditions (UP and DOWN). There is less variability close to the detection area, whereas phase inaccuracy increases with distance from the detection electrode for both conditions.

positive peak preceding the prototypical negative peak were selected for the analysis. If an additional tone was recorded between the positive peak and the maximum delay of the traveling, the wave was excluded, as it would be considered stimulated in the descending phase. For the down-phase stimulation, all the waves that were stimulated in the interval between the positive peak preceding the prototypical negative peak and the end of the traveling were considered for the analysis (see Figure 2B; selected waves are pointed with vertical arrows).

(ii) Next, TWs were classified as either small or large waves based on the amplitude of their prototypical channel. For each subject, the median of the prototypical peak amplitudes was selected as the threshold for the classification. For a topographical representation (especially for the small waves), we selected waves with an involvement higher than the 40th percentile of the involvement distribution across all the waves for each subject. Mean number of selected small and large TWs is shown in Table 2.

(iii) Finally, comparisons between ON/OFF windows and between conditions were performed as described above (see Traveling-wave selection procedure, 1, ii-iv).

3)In the final step of the analysis, we considered only the waves that traveled over the right prefrontal area, where the detection electrode was placed, and the left prefrontal area in order to evaluate lateralized local changes in traveling parameters.

(i) All the waves for which their prototypical channel was located at the top right and top left quartile of the electrode manifold, respectively, were selected for this analysis. The decreased number of resulting waves due to this restriction did not allow for a further classification into small and

large waves. We did not impose restrictions on percentage of cortical involvement. The mean number of selected TWs is shown in Table 2.

(ii) We computed the displacements, the maximum delays, and the speeds of the TWs. The displacements were computed as the total Euclidean distance from the start to endpoint of the streamlines. The maximum delays represent the time interval between the first recorded negative peak and the last recorded negative peak of the involved channels (i.e., the traveling duration). Finally, we identified the electrodes that were spanned by each streamline and the speed was computed as the ratio of the total distance traveled (i.e., the cumulative sum of all coordinates of the line) and the delay between first and last detected electrode. Grid units were converted to cm with electrode distance interpolation based on the head measurements of each individual.

Statistics

For the topographical comparisons of the traveling characteristics, we used nonparametric cluster-based statistical mapping applying a suprathreshold cluster analysis to control for multiple comparisons [12, 16, 40]. Briefly, for each topographical statistical comparison, the condition label was randomly permuted between the contrasting groups, and paired Student's *t*-tests or Spearman correlations were performed. For each permutation the maximum size of resulting clusters of neighboring electrodes reaching a *t*-value above a critical value was computed to form a cluster size distribution. From this cluster size distribution, the 97.5th percentile was defined as critical cluster size threshold. Only electrodes reaching a *t*-value beyond the critical value (CV) and located within a cluster larger than the critical cluster size threshold were considered as significant (paired Student's *t*-test: CV = 2.2, corresponding to a = .05 for the given degrees of freedom, number of permutations 1000, n = 10, Spearman correlations: CV = 0.56, number of permutations 1000, n = 10). All analyses of the sleep data and topographical statistical analyses were performed in MATLAB (R2017b, The Math- Works, Inc., Natick, Massachusetts). We used linear mixed models (LMM) with nested data structures to describe the data in our repeated measures design (lme function from nlme R package). We applied Wald Chi-squared test statistics for the description of goodness of fit of the LMM. For the LMM, the participant was treated as the random variable (varying in the intercept) and the fixed effects were the condition (UP and DOWN), the session (Stim and Sham) nested in the condition, the window (ON and OFF) nested in the session and the hemisphere (Left and Right) nested in the window. We used the maximum likelihood method for the estimation of the parameters of interest. In case of more than one variable, we performed bidirectional stepwise regression using the Akaike Information Criterion (AIC) for model comparison (stepAIC function in MASS R package). The stepwise principle for model construction is an automatic procedure of selecting the regression model that best fits the data. Initially, all the candidate predictive variables were included in the model, and then the bidirectional stepwise regression was applied in order to estimate the final model that included the variables and/or their interactions that explained best the variation of the outcome. In short, an initial model was defined only by the intercept. Next, the predictor that best predicted the outcome was selected according to highest correlation with the outcome. If this predictor improved the ability of the model to predict the outcome, then it was retained in the model. Each time a predictor was added, a removal test was made of the least useful predictor. Then a second predictor is selected by using semi-partial correlations with the outcome as a criterion. At each step, the resulting models were compared to each other using the AIC which was computed as AIC = –2(log-likelihood) + 2k, where k was the number of model parameters including the intercept and the log-likelihood was a measure of model fit. The lower the AIC the better the fit of the model. The advantage of this method is that it provides an objective way to estimate the LMM. Normality was confirmed using Shapiro-Wilk tests and thus, two-tailed paired *t*-tests were used for post-hoc comparisons (descriptive values of mean and standard error of the mean (i.e., mean ± sem) are provided). For correlation analysis, we applied the Spearman test. Statistical analysis was performed in RStudio, R-3.5.1.

Results

Statistical analysis of sleep parameters did not show any significant alterations in general sleep architecture across the different conditions (Table 3).

Topography of major characteristics of traveling waves

Topographical maps of the major characteristics of traveling waves (TWs) for all the conditions show that 1) the involvement is more prominent in broad frontal and central cortical regions (Figure 1A, upper row), 2) there is a higher probability of TWs originating in orbitofrontal and central cortical areas (Figure 1A, middle row) and 3) shorter delays in frontal areas, and larger ones in occipital regions indicate a prevalent traveling propagation from front to back (Figure 1A, bottom row) confirming results of previous studies [6, 7]. The streamline density (Figure 1C) identifies the traveling preference along the anteroposterior axis as proposed previously by Murphy et al. [7]. In general, we have shown that our adapted method confirms the major topographical characteristics and properties of TWs as well as their reproducibility across the different conditions.

Frontal increase of cortical involvement localized around the detection area in up- compared to down-phase stimulation

Topographical comparison of cortical involvement for the up-phase stimulation revealed a significant increase of 6 ± 0.3% for frontal and central cortical involvement during the stimulation in ON windows as compared to the OFF windows. (i.e., Figure 3, ΔStim in UP). For the down-phase stimulation, we observe a significant increase of 5 ± 0.1% of cortical involvement in a posterior region and a trend level decrease of 4 ± 0.3% for frontal cortical involvement (90th percentile cluster size threshold; Figure 3, ΔStim in DOWN). When comparing ON/OFF windows of the Sham sessions no differences between ON and OFF windows are observed (i.e., Figure 3, ΔSham in UP and DOWN, respectively). Comparison between Stim and Sham sessions (Figure 3, ΔStim/ΔSham) shows a significant increase of central cortical involvement of 6 ± 0.4% for the UP condition and of 5 ± 0.1% for the DOWN condition. Finally, we show that there is a significant increase of 8 ± 0.4% for frontal cortical involvement

Table 3. Sleep parameters for the three experimental sessions

	SHAM	UP	DOWN	χ^2(Df)	Pr(>χ^2)
TST (min)	187.8 ± 9.3	196.2 ± 6.2	180.5 ± 9.0	2.887(2)	0.236
SL (min)	28.1 ± 5.0	21.2 ± 3.3	30.0 ± 5.6	4.294(2)	0.117
NREM (min)	167.8 ± 7.2	171.3 ± 4.3	159.4 ± 6.8	2.509(2)	0.285
N1 (min)	8.5 ± 1.0	9.2 ± 1.7	12.4 ± 2.8	2.453(2)	0.293
N2 (min)	93.8 ± 12.4	94.1 ± 7.3	77.7 ± 7.4	5.969(2)	0.051
N3 (min)	65.5 ± 8.4	68.0 ± 9.0	69.3 ± 10.9	0.384(2)	0.825
N2+N3 (min)	159.3 ± 7.9	162.1 ± 5.4	146.9 ± 8.1	2.999(2)	0.223
REM (min)	20.0 ± 3.7	24.9 ± 4.2	21.1 ± 3.4	1.715(2)	0.424
WASO (min)	12.3 ± 5.5	12.8 ± 5.4	17.9 ± 7.1	0.6(2)	0.741
nWASO (#)	9.0 ± 1.8	9.3 ± 2.0	13.5 ± 4.9	1.448(2)	0.485
SEFF (%)	83.3 ± 4.1	86.3 ± 3.0	80.5 ± 4.2	2.124(2)	0.346

We report Chi-squared test statistics. Stimulation during up and down phase of slow waves does not affect the general sleep architecture. NREM, non-rapid eye movement sleep (stages N1 to N3); nWASO, number of awakenings after sleep onset; REM, rapid eye movement sleep; SEFF, sleep efficiency; SL, sleep latency; TST, total sleep time; WASO, wake after sleep onset.

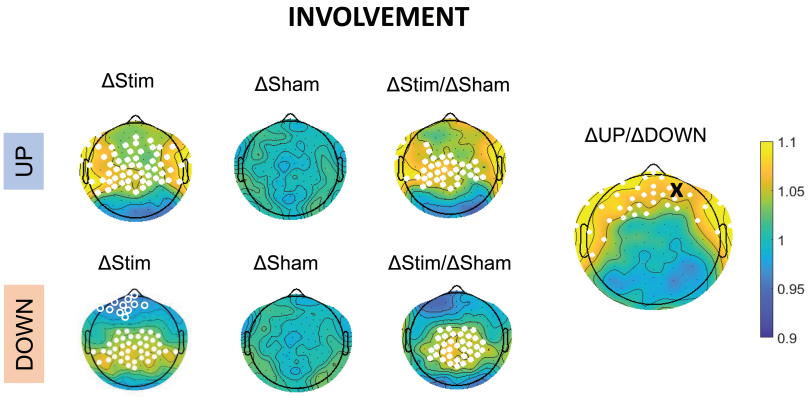

Figure 3. Overall induced changes in cortical involvement with auditory stimulation. Cortical involvement topographical comparisons of TWs that belonged in ON and OFF windows with more than three stimulations. ΔStim: ON/OFF ratio of cortical involvement for the stimulation sessions in both conditions (UP and DOWN). ΔSham: ON/OFF ratio of cortical involvement for the sham sessions in both conditions. ΔStim/ΔSham: Contrast of cortical involvement between stimulation and sham sessions by computing the ratio ΔStim/ΔSham. ΔUP/ΔDOWN: Direct comparison of the changes in involvement in UP and DOWN conditions by computing the ratio $(\Delta Stim/\Delta Sham)_{UP}/(\Delta Stim/\Delta Sham)_{DOWN}$. White dots represent significant electrodes after nonparametric cluster-based statistical comparison (97.5th percentile). White circles represent trend level cluster electrodes with a 90th percentile cluster size threshold. Black X indicates the location of the detection electrode used for slow-wave detection.

around the detection area in the UP compared to DOWN (Figure 3, ΔUP/ΔDOWN).

Small waves contribute more to the local changes in cortical involvement during up-phase stimulation whereas large waves are affected by down-phase stimulation

There is a positive correlation (all $p < .0001$) between the negative prototypical amplitude and TW involvement, which is consistent across all subjects (Supplementary Figure S1). In other words, the larger the amplitude of the prototypical channel (the channel that recorded the maximum negative peak) the higher the globality of the TW. The above observation is in agreement with the work of Siclari et al. [38] who showed that large waves are related to more global synchronicity while small waves involve circumscribed cortical regions. In order to assess whether there is a different contribution of small and large waves in the previously observed changes in frontal cortical involvement in UP compared to DOWN, we classified the TWs in small and large waves based on a median amplitude split (for mean amplitude threshold across subjects for each session see Supplementary Figure S1). We found that up-phase stimulation of small waves significantly increases frontal cortical involvement at the detection site by 8 ± 0.4%, however, up-phase stimulation of large waves does not affect cortical involvement (Figure 4A). Down-phase stimulation of large waves, on the other hand, significantly decreases cortical involvement by 5.3 ± 0.4% at the target area over the frontal cortex and increases significantly involvement by 6.6 ± 0.3% over the occipital area (Figure 4B). Stimulation of small waves during the down phase does not affect cortical involvement (Figure 4B). Therefore, the ΔUP/ΔDOWN contrast for stimulation of small waves reveals a significant local increase of cortical involvement at the detection site of 10.5 ± 0.5%. Accordingly, the ΔUP/ΔDOWN contrast for the stimulation of large waves results in a significant increase of involvement of 9.4 ± 0.6% at a left temporal region and a significant cortical involvement decrease of 6.4 ± 0.9% over the right occipital area. To exclude the possibility that the observed effects in cortical involvement in UP and DOWN are related to amplitude changes due to stimulation, we computed the Spearman correlation between the changes in involvement $((\Delta Stim/\Delta Sham)_{INV})$ and the changes in the amplitude $((\Delta Stim/\Delta Sham)_{AMP})$ at each

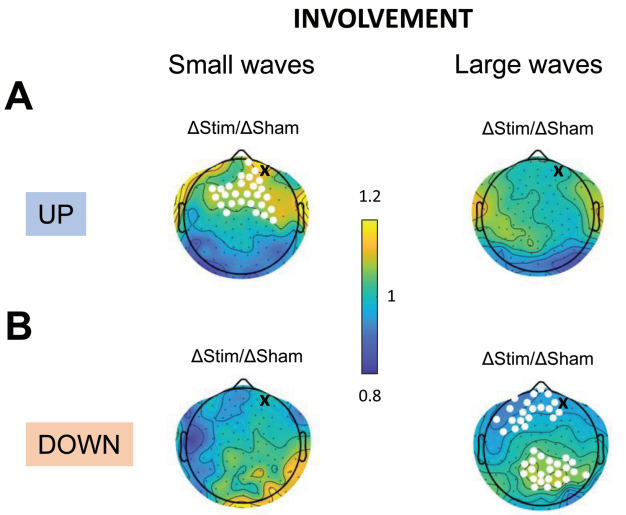

Figure 4. Higher contribution of small waves in up- and large waves in down-phase stimulation. A) ΔStim/ΔSham involvement maps for small and large waves for up-phase stimulation. White dots represent significant electrodes after nonparametric cluster-based statistical comparison. Black X indicates the location of the detection electrode used for slow-wave detection. B) ΔStim/ΔSham involvement maps for small and large waves for down-phase stimulation. White dots represent significant electrodes after nonparametric cluster-based statistical comparison. Black X indicates the location of the detection electrode used for slow-wave detection.

electrode for small and large waves, and found that there is no correlation between the two.

Distance, duration, and speed of traveling waves are differentially affected by up- and down-phase auditory stimulation

In the last step, we focused our analyses on waves traveling through the target region, namely, the right prefrontal cortex. We found during up-phase stimulation a consistent picture for all subjects showing longer displacements in Stim-ON windows (15.04 ± 0.28 cm) as compared to Sham (ON: 14.33 ± 0.33 cm, p = .05, and OFF: 14.06 ± 0.37 cm, p = .005) and Stim-OFF windows (14.13 ± 0.36 cm, p = .003). No difference was observed between Sham-ONOFF and Stim-OFF windows (Figure 5A). The ONOFF increase in displacements in Stim Up positively correlates with the ONOFF increase in involvement in Stim Up (Supplementary Figure S2B, r_s = 0.83, p = .01). No changes are observed in displacements during down-phase stimulation (Figure 5A). Figure 5B shows that maximum delays of TWs are higher in Stim-ON compared to Stim-OFF windows during up-phase stimulation (ON: 213.47 ± 3.56 ms, OFF: 207.27 ± 3.71 ms, p = .03), however, Stim-ONOFF show no differences when compared to Sham-ONOFF. On the contrary, during down-phase stimulation the traveling duration decreases during the Stim-ON windows (205.5 ± 2.6 ms) as compared to Sham (ON: 215.65 ± 1.95 ms, p = .005, OFF: 218.89 ± 1.42 ms, p < .0001) and returns to Sham levels during the Stim-OFF windows (Figure 5B). Finally, in the DOWN condition the speed of the TWs is increased by the stimulation during the Stim-ON windows (3.23 ± 0.07 m/sec) as compared to Sham (ON: 3.09 ± 0.08 m/sec, p = .09, and OFF: 2.98 ± 0.03 m/sec, p = .004) and returns to Sham levels during the Stim-OFF windows (2.94 ± 0.08 m/sec, p = .007). The speed of traveling is not affected during up-phase stimulation. No other correlations occurred among changes in the affected parameters (see Supplementary Figure S2B, C for UP and DOWN, respectively). To investigate asymmetries in traveling parameters over the prefrontal cortex we included hemisphere (left or right) into our statistical analysis. The LMMs reveal a significant effect of window (p = .01) and hemisphere (p < 2e-16) on traveling displacements (Table 4). There is a significant effect of condition (p = .0008), hemisphere (p = .004) and condition-window (p = .04) and condition-session (p = .009) interactions on the maximum delays of the TWs (Table 5) and, finally, a significant effect of condition (p < 4e-05) and window (p < 3e-05) on the traveling speeds (Table 6).

Discussion

In this work, we show for the first time how the propagation pattern of sleep slow waves is modulated by targeted phase-locked auditory stimulation during the up and down phase of slow waves in healthy young adults. Our stimulation protocol of alternating ON/OFF windows enables the investigation of the stimulation effects on the slow-wave spatiotemporal dynamics within and across the different sessions, avoiding the potential masking of effects due to night-to-night differences. We were also able to achieve a high phase accuracy and low variability in the stimulation of up- and down-phase of slow waves at the target site (Figure 2C, D). Initially, we show that our adapted method confirms the major topographical characteristics of TWs in young adults [6], namely, the predominance of frontocentral cortical involvement of TWs, their orbitofrontal and central origin as well as the propagation prevalence from frontal to more occipital and temporal cortical regions. These topographical patterns are highly reproducible across the different sessions, supporting the conclusion that they reflect cortical excitability and brain connectivity [6, 9, 10]. Further, we demonstrate that phase-targeted auditory stimulation affects key traveling parameters such as cortical involvement, TW displacement, traveling duration, and speed.

Slow-wave up-phase stimulation induces frontal cortical recruitment while down-phase stimulation seems to locally disengage cortical networks

Up-phase stimulation of slow waves of the right prefrontal area increases frontal cortical involvement compared to down-phase stimulation which tends to cause a local decrease in involvement. A large-scale computational model of the sleeping thalamocortical system predicted that an increased rate of neuronal recruitment to the up state is reflected by steep ascending slopes in the EEG, whereas high rates of neuronal decruitment to the down state are mirrored by steep descending slopes [14]. These results were further confirmed with LFP recordings in rats and human hd-EEG [15, 41]. Along these lines, our results demonstrate that up-phase stimulation locally enhances neuronal recruitment synchronous to the ongoing slow oscillation (i.e., in more channels a slow-wave peak is detected). On the contrary, down-phase stimulation seems to disengage cortical networks at the detection site which would suggest a local disruption of synchronous transition to the down state. This observation complements previous studies that demonstrated an increase

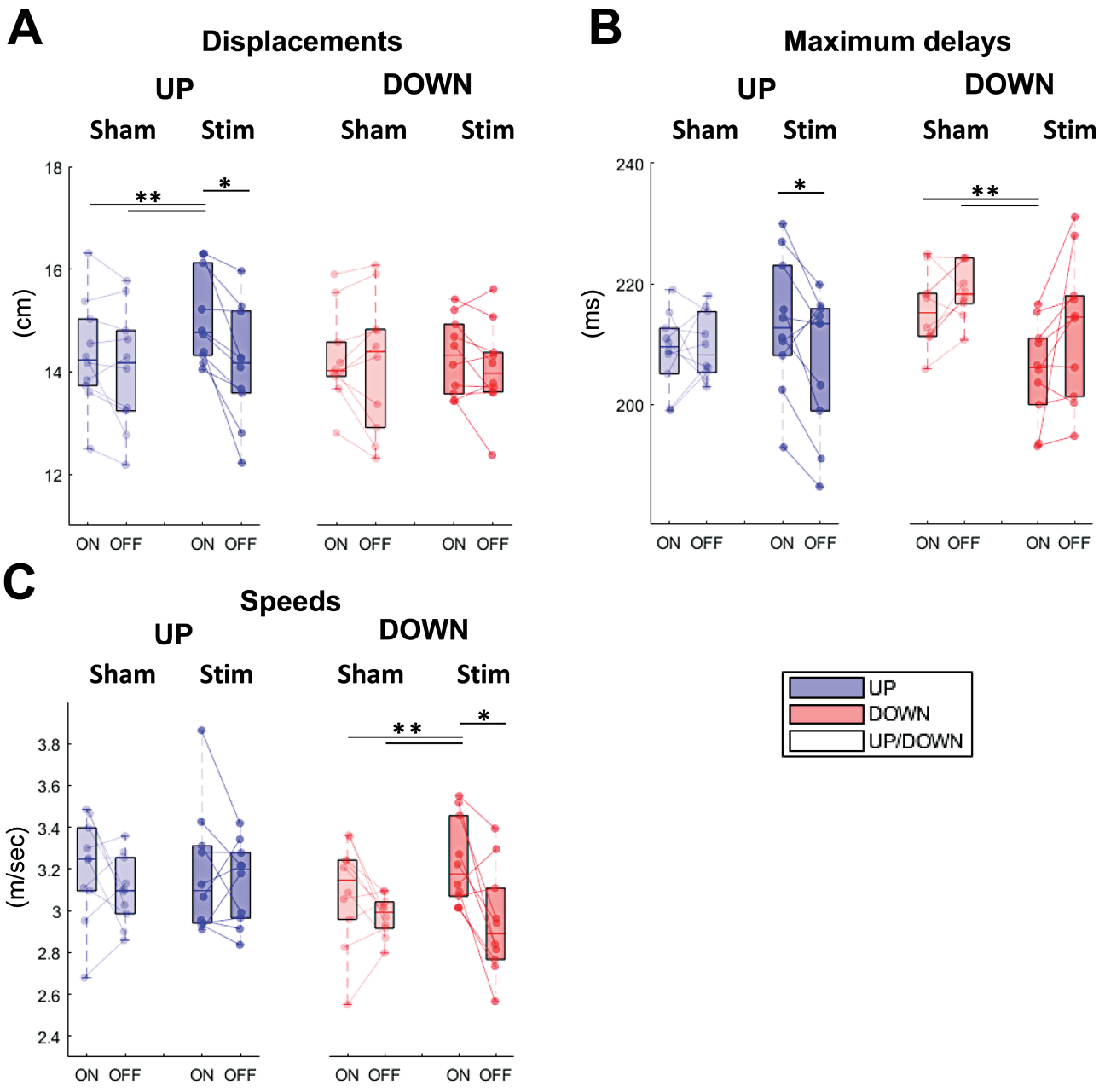

Figure 5. Displacements, maximum delays and speeds of TWs that travel through the target area. A) Mean displacements (Euclidean distance from start to end point of the longest streamline) of TWs. Displacements are increased in the ON windows during up-phase stimulation and come back to Sham levels during the OFF windows. No changes observed during down-phase stimulation (LMM: significant effect of window, $P = 0.01$ and hemisphere, $P < 2e\text{-}16$, for full model see Table 4). B) Maximum delays (total traveling duration) of TWs. Delays are higher in ON windows as compared to OFF windows during up-phase stimulation. During down-phase stimulation traveling duration decreases in ON windows as compared to Sham (LMM: significant effect of condition, hemisphere, condition-window and condition-session interaction, all $P < 0.05$, for full model see Table 5). C) Mean speed of the TWs. Up-phase stimulation does not seem to affect speed of traveling, whereas traveling speed increases in the ON windows during down-phase stimulation and returns to Sham levels in the OFF windows (LMM: significant effect of condition, $P < 4e\text{-}05$ and window, $P < 3e\text{-}05$, for full model see Table 6).

Table 4. Linear mixed model for the displacements of the TWs

	Estimate	Std. Error	χ^2(Df)	Pr(>χ^2)	95% C.I.
session	0.39	0.16	3.64(1)	0.06	0.1 to 1.03
window	–0.1	0.15	6.57(1)	**0.01**	–0.73 to –0.06
hemisphere	–2.03	0.1	398.6(1)	**< 2e-16**	0.03 to 0.8
session x window	–0.33	0.21	2.57(1)	0.1	–0.75 to 0.03

displacements ~ 1 + session + window + hemisphere + session x window + (1 | Subject/condition/session/window/hemisphere). Bold value indicates $p < 0.05$.

Table 5. Linear mixed model for the maximum delays of the TWs

	Estimate	Std. Error	χ^2(Df)	Pr(>χ^2)	95% C.I.
condition	5.03	2.25	11.32(1)	**0.0008**	0.05 to 10.01
session	1.3	1.84	2.5(1)	0.11	–2.5 to 5.07
window	–0.61	1.84	2.36(1)	0.12	–4.25 to 3.04
hemisphere	–3.66	1.3	8.28(1)	**0.004**	–6.19 to –1.13
condition x window	5.13	2.6	4.06(1)	**0.04**	–0.03 to 10.28
condition x session	–6.63	2.6	6.78(1)	**0.009**	–11.98 to –1.28

delays ~ 1 + condition + session + window + hemisphere + condition x window + condition x session + (1 | Subject/condition/session/window/hemisphere). Bold value indicates $p < 0.05$.

Table 6. Linear mixed model for the speeds of the TWs

	Estimate	Std. Error	χ^2(Df)	Pr(>χ^2)	95% C.I.
condition	–0.08	0.05	17(1)	**< 4e-05**	–0.19 to 0.03
window	–0.08	0.05	17.5(1)	**< 3e-05**	–0.18 to 0.01
condition x window	–0.12	0.07	3.04(1)	0.08	–0.25 to 0.02

speeds ~ 1 + condition + window + condition x window + (1 | Subject/condition/session/window/hemisphere). Bold value indicates $p < 0.05$.

in slow-wave amplitude and SWA after auditory stimulation at the ascending phase of slow waves [22, 23, 42]. Conversely, local disengagement of cortical regions due to down-phase stimulation (i.e., fewer channels are detecting a slow-wave peak) would be in agreement with the local reduction of SWA close to the detection electrode observed in [16] as well as with the increase of the ensuing ascending slope, further supporting the disruption of synchronous decruitment to the down state and a rapid transition to depolarization. In summary, the application of targeted phase-locked auditory stimulation results in local changes in cortical involvement. Future experiments need to determine the causal relationship between the detection electrode and these local changes, namely, whether targeting another cortical site would lead to local changes in the corresponding region.

Different contributions of small and large waves

As a further investigation of local effects, we concentrated on TWs during which a stimulation took place. We show that there is a significant positive correlation between the negative amplitude of the prototypical channel and the involvement of TWs confirming previous results [37, 38]. Further classification into small- and large-amplitude waves reveals that small waves have a higher contribution to the local changes observed in frontal cortical involvement during up-phase stimulation as compared to the large ones. On the contrary, down-phase stimulation seems to be more efficient in locally reducing cortical involvement of large waves. These changes in involvement do not correlate with any changes in slow-wave amplitudes, implying a specific effect of the stimulation on this traveling parameter.

Although sleep is considered a global phenomenon, it is well established that its regulation and organization emerges from local network interactions [43]. Indeed, some brain regions can be in the active on state, whereas simultaneously, other brain regions are in a silent off state [2]. In addition, small-amplitude slow waves in the EEG presumably represent local waves, occurring out of phase across different brain regions, as opposed to large-amplitude global waves that are in phase across the cortex. Along these lines, two distinct synchronization processes, at the falling asleep period were proposed [38], which were further identified during stable NREM sleep [37]. Type I slow waves are organized by a "bottom-up" synchronization mechanism mediated by subcortical structures. They are typically large, steep, and involve a broad frontomedial region(more global). Type II slow waves arise from cortico-cortical synchronization. They have lower amplitudes, less steep slopes, and recruit circumscribed cortical regions (more local). Accordingly, the fact that small waves are responsible for the regional changes observed in involvement during up-phase stimulation indicates that targeting acoustic stimuli to the up-phase, presumably associated with neuronal activity, seems to entrain local slow waves generated via cortico-cortical connections at the stimulation site. Contrariwise, down-phase stimulation appears to interact with the silent off periods of large, thalamo-cortical slow waves, which seem to get redistributed from anterior to more posterior regions. Specifically, stimuli targeting the down phase of slow waves seem to abolish the synchronous transition to the down state resulting in reduced involvement in the target area, whereas they emerge to a larger extent in more posterior regions. Alternatively, considering that larger waves travel at longer distances and that the distribution of negative peaks highly correlates with the distribution of ensuing positive peaks [6], the question arises whether, while frontal regions are in the down state, posterior regions are simultaneously in the on state and, thus, stimulation is targeted at the ascending phase of waves over the occipital cortex causing the observed increase in involvement. This interpretation is however speculative, as the spatiotemporal propagation of the acoustic stimuli is not known. Combining intracranial recordings with targeted auditory stimulation is needed to test these interpretations. Further alternative explanations may account for the observed effect. For example, the stimulation effects may depend merely on the size of slow waves indicating a floor/ceiling effect. More precisely, entraining slow waves by up-phase stimulation might be more efficient when targeting small waves that show less synchronicity and, thus, there is room for such an enhancement (i.e., floor effect), while synchronicity in large waves might be saturated, thus, further

recruitment cannot be promoted (i.e., ceiling effect) and vice versa.

Up-phase stimulation promotes and down-phase stimulation interferes with slow-wave traveling

For our final analysis, aiming at elucidating the direct effect of auditory stimulation on the propagation pattern of targeted waves, we assessed the traveling parameters of TWs that were detected in the right prefrontal area. Up-phase stimulation causes a prolongation of the TW propagation which correlates with the increase in involvement, as found before (see Supplementary Figure S2A, B and [9]). Moreover, our results show an increase in traveling duration whereas speed remained unaffected. Down-phase stimulation, on the other hand, does not seem to influence the traveling distance, however, TWs become shorter in duration and faster. Importantly, hemisphere is a significant factor for traveling displacements and delays, however, not for traveling speeds, indicating that auditory stimulation targeted at the right prefrontal cortical area causes lateralized local changes in the slow-wave traveling parameters.

Recently it was shown that while cortical involvement and traveling speed are not affected by age, slow-oscillation propagation distance increases with age indicating increased functional connectivity throughout development [9]. In schizophrenia that is characterized by dysconnectivity among functional brain regions [44, 45], patients displayed reduced traveling distances whereas speed did not differ from that of healthy controls. Along these lines, phase-locked stimulation at the up phase of slow waves seems to regionally promote synchronous activity to neighboring cortical structures through cortico-cortical connections and, thus, increase the traveling distance. Interestingly, the increased traveling duration did not correlate with the increase in involvement or in displacements, which might indicate longer sustained periods of synchronous bistable states due to up-phase stimulation. Conversely, during down-phase stimulation traveling duration was decreased and accompanied by an increase in speed. Massimini et al. showed that, during a traveling cycle, the timing of the negative peak highly correlates with the timing of the ensuing positive zero-crossing [6], hence suggesting that traveling speed might reflect how fast neurons leave the hyperpolarization phase and enter the on state. Altogether, these results indicate that down-phase stimulation might interrupt the synchronous transition to the down state, and thus, reduce the duration of the hyperpolarized phase, and induce neuronal excitation and a faster transition to depolarization. Of course, all these interpretations remain speculative, and simultaneous intracranial and/or unit firing and surface recordings would be needed to support or dispute them.

Conclusion and outlook

We provide first critical insights into the mechanism underlying the potential of auditory stimulation to manipulate slow waves during sleep. Importantly, we provide initial evidence for different mechanisms underlying the effects of up- and down-phase stimulation of slow waves. Such information may prove critical for the future development of this technology for therapeutic application. As neuromodulation during sleep holds great potential in various neurological and psychiatric disorders [10, 28, 46–52] a thorough understanding is needed to address the specific needs of the different disorders and potentially allow personalization of the therapeutic interventions. Finally, a limitation of our study is the small sample size and it will be interesting to see the application of our methods and ideas of analysis to study cortical connectivity and excitability in the future. Additionally, an interesting future direction would be the assessment of the described changes in markers of excitability and connectivity with respect to overnight behavioral outcomes.

Supplementary material

Supplementary material is available at *SLEEP* online.

Funding

The current study was supported by research grants from the Schweizerische Hirnstiftung, the ETH Zürich Foundation, and the Swiss National Science Foundation (320030_179443).

Acknowledgments

This work was conducted as part of the SleepLoop Flagship of Hochschulmedizin Zürich. We thank all of our participants for taking part in this study. We appreciate the helpful discussions with numerous SleepLoop consortium members.

Disclosure Statement

None declared.

References

1. Vyazovskiy VV, *et al*. Cortical firing and sleep homeostasis. *Neuron*. 2009;**63**(6):865–878.
2. Nir Y, *et al*. Regional slow waves and spindles in human sleep. *Neuron*. 2011;**70**(1):153–169.
3. Steriade M, *et al*. The slow (< 1 Hz) oscillation in reticular thalamic and thalamocortical neurons: scenario of sleep rhythm generation in interacting thalamic and neocortical networks. *J Neurosci*. 1993;**13**(8):3284–3299.
4. Timofeev I, *et al*. Origin of slow cortical oscillations in deafferented cortical slabs. *Cereb Cortex*. 2000;**10**(12):1185–1199.
5. Crunelli V, *et al*. The slow (<1 Hz) rhythm of non-REM sleep: a dialogue between three cardinal oscillators. *Nat Neurosci*. 2010;**13**(1):9–17.
6. Massimini M, *et al*. The sleep slow oscillation as a traveling wave. *J Neurosci*. 2004;**24**(31):6862–6870.
7. Murphy M, *et al*. Source modeling sleep slow waves. *Proc Natl Acad Sci U S A*. 2009;**106**(5):1608–1613.
8. Avvenuti G, *et al*. Integrity of corpus callosum is essential for the cross-hemispheric propagation of sleep slow waves: a high-density EEG study in split-brain patients. *J Neurosci*. 2020;**40**(29):5589–5603.
9. Kurth S, *et al*. Traveling slow oscillations during sleep: a marker of brain connectivity in childhood. *Sleep*. 2017;**40**(9). doi:10.1093/sleep/zsx121
10. Castelnovo A, *et al*. Slow wave oscillations in Schizophrenia First-Degree Relatives: a confirmatory analysis and

feasibility study on slow wave traveling. *Schizophr Res*. 2020;**221**:37–43.
11. Esser SK, *et al*. A direct demonstration of cortical LTP in humans: a combined TMS/EEG study. *Brain Res Bull*. 2006;**69**(1):86–94.
12. Huber R, *et al*. Local sleep and learning. *Nature*. 2004;**430**(6995):78–81.
13. Tononi G, *et al*. Sleep and the price of plasticity: from synaptic and cellular homeostasis to memory consolidation and integration. *Neuron*. 2014;**81**(1):12–34.
14. Esser SK, *et al*. Sleep homeostasis and cortical synchronization: I. Modeling the effects of synaptic strength on sleep slow waves. *Sleep*. 2007;**30**(12):1617–1630.doi
15. Riedner BA, *et al*. Sleep homeostasis and cortical synchronization: III. A high-density EEG study of sleep slow waves in humans. *Sleep*. 2007;**30**(12):1643–1657.doi: 10.1093/sleep/30.12.1617
16. Fattinger S, *et al*. Deep sleep maintains learning efficiency of the human brain. *Nat Commun*. 2017;**8**:1–13.
17. Huber R, *et al*. Arm immobilization causes cortical plastic changes and locally decreases sleep slow wave activity. *Nat Neurosci*. 2006;**9**(9):1169–1176.
18. Rasch B, *et al*. About sleep's role in memory. *Physiol Rev*. 2013;**93**(2):681–766.
19. Born J, *et al*. Sleep to remember. *Neuroscientist*. 2006;**12**(5):410–424.
20. Ngo HV, *et al*. Auditory closed-loop stimulation of the sleep slow oscillation enhances memory. *Neuron*. 2013;**78**(3):545–553.
21. Ngo HV, *et al*. Driving sleep slow oscillations by auditory closed-loop stimulation-a self-limiting process. *J Neurosci*. 2015;**35**(17):6630–6638.
22. Papalambros NA, *et al*. Acoustic enhancement of sleep slow oscillations and concomitant memory improvement in older adults. *Front Hum Neurosci*. 2017;**11**:109.
23. Ong JL, *et al*. Effects of phase-locked acoustic stimulation during a nap on EEG spectra and declarative memory consolidation. *Sleep Med*. 2016;**20**:88–97.
24. Ong JL, *et al*. Auditory stimulation of sleep slow oscillations modulates subsequent memory encoding through altered hippocampal function. *Sleep*. 2018;**41**(5).doi: 10.1093/sleep/zsy031
25. Besedovsky L, *et al*. Auditory closed-loop stimulation of EEG slow oscillations strengthens sleep and signs of its immune-supportive function. *Nat Commun*. 2017;**8**(1):1–8. doi: 10.1038/s41467-017-02170-3
26. Grimaldi D, *et al*. Strengthening sleep-autonomic interaction via acoustic enhancement of slow oscillations. *Sleep*. 2019;**42**(5) .doi:10.1093/sleep/zsz036
27. Papalambros NA, *et al*. Acoustic enhancement of sleep slow oscillations in mild cognitive impairment. *Ann Clin Transl Neurol*. 2019;**6**(7):1191–1201.
28. Prehn-Kristensen A, *et al*. Acoustic closed-loop stimulation during sleep improves consolidation of reward-related memory information in healthy children but not in children with attention-deficit hyperactivity disorder. *Sleep*. 2020;**43**(8). doi: 10.1093/sleep/zsaa017
29. Fattinger S, *et al*. Closed-loop acoustic stimulation during sleep in children with epilepsy: a hypothesis-driven novel approach to interact with spike-wave activity and pilot data assessing feasibility. *Front Hum Neurosci*. 2019;**13**:1–10.
30. Ferster ML, *et al*. Configurable mobile system for autonomous high-quality sleep monitoring and closed-loop acoustic stimulation. *IEEE Sensors Lett*. 2019;**3**(5):1–4.
31. Delorme A, *et al*. EEGLAB : an open source toolbox for analysis of single-trial EEG dynamics including independent component analysis. *J Neurosci Methods*. 2004;**134**(1):9–21.
32. Berry RB, *et al*. AASM scoring manual updates for 2017 (Version 2.4). *J Clin Sleep Med*. 2017;**13**(5):665–666.
33. Huber R, *et al*. Exposure to pulsed high-frequency electromagnetic field during waking affects human sleep EEG. *Neuroreport*. 2000;**11**(15):3321–3325.
34. Mensen A, *et al*. Optimizing detection and analysis of slow waves in sleep EEG. *J Neurosci Methods*. 2016;**274**:1–12.
35. Duckrow RB, *et al*. Coherence of the electroencephalogram during the first sleep cycle. *Clin Neurophysiol*. 2005;**116**(5):1088–1095.
36. Rocca D, *et al*. Human brain distinctiveness based on EEG spectral coherence connectivity. *IEEE Trans Biomed Eng*. 2014;**61**(9):2406–2412.
37. Bernardi G, *et al*. Local and widespread slow waves in stable NREM sleep: evidence for distinct regulation mechanisms. *Front Hum Neurosci*. 2018;**12**:1–13.
38. Siclari F, *et al*. Two distinct synchronization processes in the transition to sleep: a high-density electroencephalographic study. *Sleep*. 2014;**37**(10):1621–1637.doi: 10.5665/sleep/4070
39. Welch PD. The use of fast Fourier transform for the estimation of power spectra: a method based on time averaging over short, modified periodograms. *IEEE Trans Audio Electroacoust*. 1967;**15**(2):70–73.
40. Nichols T, *et al*. Nonparametric permutation tests for functional neuroimaging. *Hum Brain Funct Second Ed*. 2003;**25**:887–910.
41. Vyazovskiy VV, *et al*. Sleep homeostasis and cortical synchronization: II. A local field potential study of sleep slow waves in the rat. *Sleep*. 2008;**30**:1631–1642. doi:10.1093/sleep/30.12.1631
42. Krugliakova E, *et al*. Changes in cross-frequency coupling following closed-loop auditory stimulation in non-rapid eye movement sleep. *Sci Rep*. 2020;**10**(1):1–12. doi:10.1038/s41598-020-67392-w
43. Krueger JM, *et al*. Sleep as a fundamental property of neuronal assemblies. *Nat Rev Neurosci*. 2008;**9**(12):910–919.
44. Lynall ME, *et al*. Functional connectivity and brain networks in schizophrenia. *J Neurosci*. 2010;**30**(28):9477–9487.
45. Fitzsimmons J, *et al*. Review of functional and anatomical brain connectivity findings in schizophrenia. *Curr Opin Psychiatry*. 2013;**26**(2):172–187.
46. Schreiner SJ, *et al*. Slow-wave sleep and motor progression in Parkinson disease. *Ann Neurol*. 2019;**85**(5):765–770.
47. Mander BA, *et al*. β-amyloid disrupts human NREM slow waves and related hippocampus-dependent memory consolidation. *Nat Neurosci*. 2015;**18**(7):1051–1057.
48. Lee YF, *et al*. Slow wave sleep is a promising intervention target for Alzheimer's disease. *Front Neurosci*. 2020;**14**:1–11.
49. D'Agostino A, *et al*. Sleep endophenotypes of schizophrenia: slow waves and sleep spindles in unaffected first-degree relatives. *NPJ Schizophr*. 2018;**4**(1):1–8.
50. Tesler N, *et al*. Increased frontal sleep slow wave activity in adolescents with major depression. *Neuroimage Clin*. 2016;**10**:250–256.
51. Boly M, *et al*. Altered sleep homeostasis correlates with cognitive impairment in patients with focal epilepsy. *Brain*. 2017;**140**(4):1026–1040.
52. Kang X, *et al*. Quantitative spatio-temporal characterization of epileptic spikes using high density EEG: differences between NREM sleep and REM sleep. *Sci Rep*. 2020;**10**(1):1673.